Quantification of aerosol signal in GOES 8 visible imagery over the United States

Kenneth R. Knapp

Cooperative Institute for Research in the Atmosphere, Camp Springs, Maryland, USA

Received 12 December 2001; revised 6 March 2002; accepted 7 March 2002; published 23 October 2002.

[1] Changes in the top-of-the-atmosphere reflectance due to variations in the aerosol optical depth (τ) make retrieving τ from satellite possible. This aerosol signal is greatest for non-absorbing aerosol over dark surfaces and is least (often less than zero) for absorbing aerosols over bright surfaces. In general, previous aerosol retrieval research has been in regions where the signal is known to be large, for example, aerosol over ocean or biomass burning over heavily vegetated land. This study, however, looks at the aerosol signal and its variation over North America to determine when and where τ retrieval is possible. The results show that the aerosol signal is sufficiently large for τ retrieval over most of the sites studied; exceptions are located in the southwestern United States where the surface reflectance is large. Further, this aerosol signal closely corresponds with radiative transfer simulations, which suggests that aerosol optical depth retrieval over North America and the adjoining oceans is possible from geostationary orbit. The implication is that timely (e.g., 30 min intervals) observations of aerosol are possible. Such observations could aid research efforts in pollutant transport, air quality forecasting, and wildfire monitoring. *INDEX TERMS:* 0305 Atmospheric Composition and Structure: Aerosols and particles (0345, 4801); 0345 Atmospheric Composition and Structure: Pollution—urban and regional (0305); 3359 Meteorology and Atmospheric Dynamics: Radiative processes; 3360 Meteorology and Atmospheric Dynamics: Remote sensing; *KEYWORDS:* aerosol, remote sensing, GOES, optical depth

Citation: Knapp, K. R., Quantification of aerosol signal in GOES 8 visible imagery over the United States, *J. Geophys. Res.*, *107*(D20), 4426, doi:10.1029/2001JD002001, 2002.

1. Introduction

[2] Aerosols play an important role in numerous scientific processes and societal issues. For instance, aerosols directly interact with solar radiation, redistributing the solar heating, which can have an effect on weather forecasts and climate analyses. Also, the air quality community could use satellite aerosol observations to monitor the growth and dispersion of air pollution episodes, whose presence can affect human health. Additionally, the dispersion of smoke from wildfires can be important to the aircraft efforts fighting the fires as well as to populations downwind. Thus the daily monitoring of aerosols over land is essential. While *Kaufman et al.* [2000] demonstrate little bias in comparing once per day observations with daily averages, they do show variations in aerosol optical depth (τ) of 10% or more during the day, which suggests multiple τ retrievals per day could prove beneficial. Since this frequency is not available from polar orbiting satellites, it is prudent to look to geostationary instruments.

[3] However, aerosol remote sensing is predominantly a polar orbit science. Numerous instruments aboard polar orbiting satellites have been used for aerosol remote sensing, including the Advanced Very High Resolution Radiometer (AVHRR), the Coastal Zone Color Scanner (CZCS), Landsat, the Total Ozone Mapping Spectrometer (TOMS), the Moderate Resolution Spectroradiometer (MODIS), the Multiangle Imaging Spectroradiometer (MISR), the Polarization and Directionality of Earth's Reflectance (POLDER), and Sea-viewing Wide Field-of-view Sensor (SeaWiFS). (*King et al.* [1999] provide a thorough review of tropospheric aerosol satellite remote sensing). Research from geostationary orbit is more limited because there are fewer meteorological geostationary satellites and the orbit limits the satellite field of view to only a portion of the Earth.

[4] Also, it is clear from the above applications that retrievals over both land and ocean are needed. Yet τ retrievals over land generally have larger errors than those over ocean. This is because land is brighter, more heterogeneous, and more variable in time. Particularly, the brighter reflectance of the land reduces the aerosol signal relative to the surface. In fact, for bright surfaces, aerosols actually decrease the top-of-the-atmosphere solar reflectance [*Kaufman*, 1987]. Also, the visible reflectance of the ocean is better described than the bidirectional reflectance distribution function (BRDF) of land, which varies both temporally and spatially. Therefore, while aerosol remote sensing algorithms for oceans abound [e.g., *Durkee et al.*, 1991; *Higurashi et al.*, 2000; *Mishchenko and Travis*, 1997; *Stowe et al.*, 1992], they are more limited over land [e.g., *Flowerdew and Haigh*, 1996; *Kaufman et al.*, 1997a]. However, aerosol information over land is beneficial because numerous aerosol sources, partic-

0148-0227/02/2001JD002001$09.00

ularly those with anthropogenic influences, are located over the continents. Aerosol remote sensing over land does include research using: AVHRR [*Bruegge et al.*, 1992; *Fraser*, 1993], the Geostationary Observational Environmental Satellite (GOES) [*Fraser et al.*, 1984], or Landsat [*Conel*, 1990]. However, these studies have limited scope, applicability, and validation. More recently, newer instruments and methods have allowed the development of τ retrieval algorithms which are more global in nature, such as the Along-track Scanning Radiometer (ATSR) [*Veefkind and de Leeuw*, 1998], POLDER [*Herman et al.*, 1997b], TOMS [*Herman et al.*, 1997a], and MODIS [*Kaufman et al.*, 1997a].

[5] Aerosol research from geostationary satellites is slowly building toward routine τ retrieval processing. While studies have shown the ability of sensing aerosols over ocean [*Griggs*, 1979; *Norton et al.*, 1980], *Lyons et al.* [1977] recognize the importance of geostationary imagery in qualitatively analyzing pollutant transport over the eastern United States. *Fraser et al.* [1984] further this research by quantitatively estimating the aerosol mass and transport over the United States using GOES. Later, *Tsonis and Leaitch* [1986] estimated the minimum detectable aerosol optical depth over central Ontario, Canada, to be 0.065. Also, it has been shown that aerosols over desert regions can be sensed using infrared wavelengths [*Legrand et al.*, 1989]. More recently, research by *Knapp et al.* [2002] and *Zhang and Christopher* [2001] have demonstrated the ability to monitor biomass burning in South America from GOES 8. Nonetheless, the South American case is simplistic because of the large aerosol signal associated with biomass burning (smoke plumes often have optical depths greater than 1) and the dark uniform background of the vegetated areas in which the burning occurs. The ability of GOES to sense aerosol over a variety of surface types and at numerous illumination conditions is yet to be shown. Therefore this study investigates the ability of GOES to detect summertime aerosol conditions for locations scattered across the United States.

[6] Aerosol signal is herein defined as the response of the detected solar reflectance at the top-of-the-atmosphere (ρ_{sat}) to changes in τ. This study concentrates on the aerosol signal over North America as detectable from geostationary satellites, particularly GOES 8. The cloud-free satellite-detected solar reflectance is compared to collocated ground-based observations of τ. This observed aerosol signal is then compared to a simulated signal from radiative transfer, which confirms that the signal is due to aerosol. Results show that aerosol optical depth can be retrieved over much of North America from a single geostationary satellite at a temporal resolution of 30 min (but the temporal resolution depends only on the operational constraints of the instrument). Given that geostationary-based retrievals can provide timely information for such applications as air quality research, these results are encouraging.

2. Determination of Aerosol Signal

[7] The first step in this research is to determine the aerosol signal. This is done by comparing cloud-free satellite observations with ground-based measurements of aerosol optical depth. Linear regression is used to determine the aerosol signal, because the relationship between satellite-detected reflectance (ρ_{sat}) and aerosol optical depth (τ) is primarily linear. Any nonlinearity, which can occur for larger atmospheric path lengths, is not considered herein (but would be accounted for in a retrieval by a radiative transfer model). The linear regression slope defines the aerosol signal by quantifying the response of ρ_{sat} to τ. In the next section, the aerosol signal is simulated using a radiative transfer model and compared to the aerosol signal observed.

2.1. Description of GOES and AERONET Data

[8] Observations from the GOES 8 visible sensor are used to sense aerosol from geostationary orbit. The time period for the comparisons is June through August 2001. Data from channel 1 (the visible, 0.52–0.72 μm) are used to compare with ground-based τ observations while information from channels 2 (3.78–4.03 μm), 4 (10.2–11.2 μm), and 5 (11.5–12.5 μm) are used to remove clouds from the comparisons using spectral difference and spatial uniformity tests. The GOES imagery used in this study was available at 30 min intervals. The visible data were also calibrated to account for instrument degradation in a similar manner to *Knapp and Vonder Haar* [1999]; the degradation for August 2001 was 57% of the prelaunch instrument responsivity value. The GOES-observed reflectance, ρ_{sat}, is calculated from the visible channel radiance (L) via

$$\rho_{sat} = \frac{\pi L}{\delta(D)\mu_o F_o}, \tag{1}$$

where δ is the Earth-Sun distance correction for day of year D, μ_o is the cosine of the solar zenith angle, and F_o is the solar flux weighted by the instrument spectral response. Further details of the GOES Imager can be found in the work of *Ellrod et al.* [1998] and *Menzel and Purdom* [1994].

[9] Ground-based observations of τ are available from the Aerosol Robotic Network (AERONET), which monitors aerosol optical depth at more than 100 sites around the globe. AERONET is a network of Sun-sky radiometers which report the spectral aerosol optical depth as well as some information about the aerosol optical properties [*Dubovik and King*, 2000; *Holben et al.*, 1998]. At 33 sites around the contiguous United States and Canada, level 1.5 AERONET data (that is, cloud-screened data without postcalibration) are interpolated to 0.55 μm for comparison with GOES data. The interpolation to 0.55 μm allows direct comparison with the radiative transfer model simulations described below, and it is performed in a similar manner to *Zhao et al.* [2002]. The accuracy of AERONET is $\pm$0.02 once postcalibrated (i.e., level 2.0), thus it is likely larger herein (without the postcalibration). The sites are listed in Table 1, where the names used are from the AERONET data archive. These same sites are also shown in Figure 1 with a cloud-free composite visible reflectance from GOES 8 (that is, the lowest ρ_{sat} observed in a 30-day period) demonstrating the variability of the surface brightness at the sites. Apparent from the spatial distortion of the map, the satellite view zenith angle (θ) increases toward the northwest United States. Overall, θ varies from 23° at La Paguera to 73° at Saturn Island.

[10] Comparisons of GOES ρ_{sat} with AERONET τ are made with collocated observations in time and space. GOES observations are averaged over a 12 $\times$ 12 km^2 region (i.e.,

Table 1. Summary Statistics for the Determination of Aerosol Signal at AERONET Sites[a]

Site	N	$\hat{m}$	Median SNR	$m < 0$, %	SNR > 1, %	$\hat{\rho}_{sfc}$
Bondville	20	0.074	1.36	0	65	0.087
Boulder	17	0.119	0.50	6	29	0.127
Bermuda	18	0.102	1.65	0	89	0.018
Bratts Lake	19	0.189	0.63	0	21	0.146
CARTEL	17	0.070	0.87	23	41	0.090
COVE	21	0.072	4.96	0	81	0.014
Cart Site	19	0.127	1.51	0	74	0.122
Chequamegon	19	0.128	1.59	0	79	0.063
Dry Tortugas	21	0.079	2.59	0	90	0.022
Egbert	21	0.074	2.18	0	81	0.092
GISS	20	0.077	2.04	0	80	0.073
GSFC	21	0.090	3.18	0	95	0.074
HJAndrews	16	0.148	2.86	0	62	0.069
Harvard Forest	14	0.071	0.79	6	35	0.069
Howland	19	0.071	1.56	0	63	0.065
KONZA EDC	20	0.087	1.97	0	95	0.094
La Jolla	9	0.089	0.92	0	44	0.018
La Paguera	17	0.067	1.38	0	70	0.083
Maricopa	7	−0.148	−0.52	71	14	0.280
Mexico City	9	0.062	1.09	0	55	0.114
Missoula	8	0.166	1.00	0	38	0.116
Mont Joli	16	0.076	1.20	0	62	0.013
Oyster	4	0.092	1.75	0	100	0.069
Philadelphia	17	0.096	2.63	0	100	0.078
Railroad Valley	3	0.074	0.16	33	0	0.190
Rimrock	19	0.251	1.31	5	63	0.127
Rogers Dry Lake	18	0.129	1.05	6	50	0.220
Saturn Island	19	0.200	1.88	5	63	0.031
Sevilleta	18	0.006	0.02	50	0	0.188
Sioux Fall	19	0.075	1.03	0	52.6	0.101
Walker Branch	15	0.077	3.00	7	93	0.060
Wallops	20	0.072	4.68	0	95	0.071
Waskesiu	18	0.163	1.43	5	78	0.056

[a] Statistics include number of comparisons available per day (N), median aerosol signal ($\hat{m}$), median signal-to-noise ratio (SNR), percentage of comparisons with $m < 0$, percentage of comparisons with SNR > 1, and the median Lambertian reflectance ($\hat{\rho}_{sfc}$).

12 × 12 visible pixels), then collocated in time with an AERONET τ observation that is within ±15 min of the image. These matchups are collected for each time of day during the 90 days of the study. The following is a description of the error characteristics used in analyzing the observed aerosol signal at an arbitrary site, followed by a summary of the same statistics at all sites.

2.2. Example of a GOES-AERONET Comparison at Konza EOS Data Center (EDC)

[11] Figure 2a shows an example of a comparison of GOES ρ_{sat} with AERONET τ demonstrating an aerosol signal for the Konza EDC site using observations from 2145 UTC; the solid line is the linear regression. For the 24 points (representing 24 days at the same time of day), there is high correlation (0.93) and the linear regression slope (m) and offset (b) are 0.123 and 0.090, respectively. Time series of diurnal m and b values are plotted in Figures 2b and 2c, respectively, since a similar comparison is available for each GOES observation time. The observed aerosol signal for Konza EDC (Figure 2b) shows larger aerosol signal as the sun sets (i.e., after 2100 UTC). The comparison also shows some noise in m, for example, observations at 1415 and 1815 UTC deviate from the otherwise smooth relationship.

[12] To quantify the noise in these comparisons and its possible impact on retrievals, statistics from the linear regression are used. First, the uncertainty of the aerosol signal (Δm) is quantified via [*Kachigan*, 1986] as

$$\Delta m = \frac{\varepsilon_\rho T(99\%, n)}{\sqrt{\sum(\tau - \bar{\tau})^2}}, \tag{2}$$

where $\bar{\tau}$ is the mean τ for each comparison, T is the Student's T-distribution for a 99% confidence limit with n comparison points, and the standard error of estimate (ε_ρ) is calculated as

$$\varepsilon_\rho = \sqrt{\frac{\sum(\rho_{sat} - \rho_{sat-LR})^2}{n-2}}, \tag{3}$$

where the summation is over the n observations in each comparison. For example, for Konza EDC at 2145 UTC (Figure 2a), $\varepsilon_\rho = 0.0042$ and $\Delta m = 0.026$. So, where the uncertainty is large, particularly where $\Delta m > m$, the aerosol signal is uncertain and likely not retrievable. Thus the signal-to-noise ratio (SNR) is defined as $m/\Delta m$. In this case, the SNR is 4.73.

[13] Also, ε_ρ can be converted to a noise estimate in terms of τ (ε_τ) via

$$\varepsilon_\tau = \varepsilon_\rho / m; \tag{4}$$

$\varepsilon_\tau = 0.034$ for Figure 2a. This noise estimate not only describes the quality of linear regression fit, but also describes the noise involved in comparing a satellite observation with a ground-based measurement of τ. It is analogous to how accurate a τ retrieval could be. As such, it is an optimal estimate of retrieval accuracy which assumes that a retrieval uses the exact surface reflectance and aerosol signal.

[14] Overall, the aerosol signal is well-defined at Konza EDC. The median aerosol signal is 0.087 (compare with Table 1) and more importantly the SNR is greater than 1 (i.e., the signal is larger than the uncertainty) 95% of the day. While the median ε_τ is 0.07, ε_τ shows a temporal trend (Figure 2d) where values are large (∼0.1) before 1800 UTC and lower thereafter. This suggests that afternoon retrievals would be more accurate due to some dependence of ε_τ on viewing geometry, which is discussed later.

[15] Noise in the comparisons, which causes Δm and ε_τ to increase, occurs when changes in ρ_{sat} are not caused by changes in τ. This occurs from day-to-day variations in aerosol type (i.e., size distribution and composition), gaseous absorption (H_2O or O_3), surface reflectance, cloud and cloud shadow contamination, and satellite registration (i.e., navigation errors). In particular, comparisons located in regions of vegetation, such as the Cart Site, encounter seasonal growth possibly causing the surface reflectance to change during the study period (June through August).

2.3. Effect of Surface Changes

[16] To see whether possible surface changes are affecting this analysis, the aerosol signal analysis at the Cart Site is separated by month in Figure 3 for three times of day (1615, 1645, and 1715 UTC). The solid line in each figure shows the linear regression that was used in the analysis described above; observations from June, July and August are denoted by pluses, triangles and squares (respectively). The GOES-observed reflectances are increasing in time: June observations are the darkest and reflectance values increase each

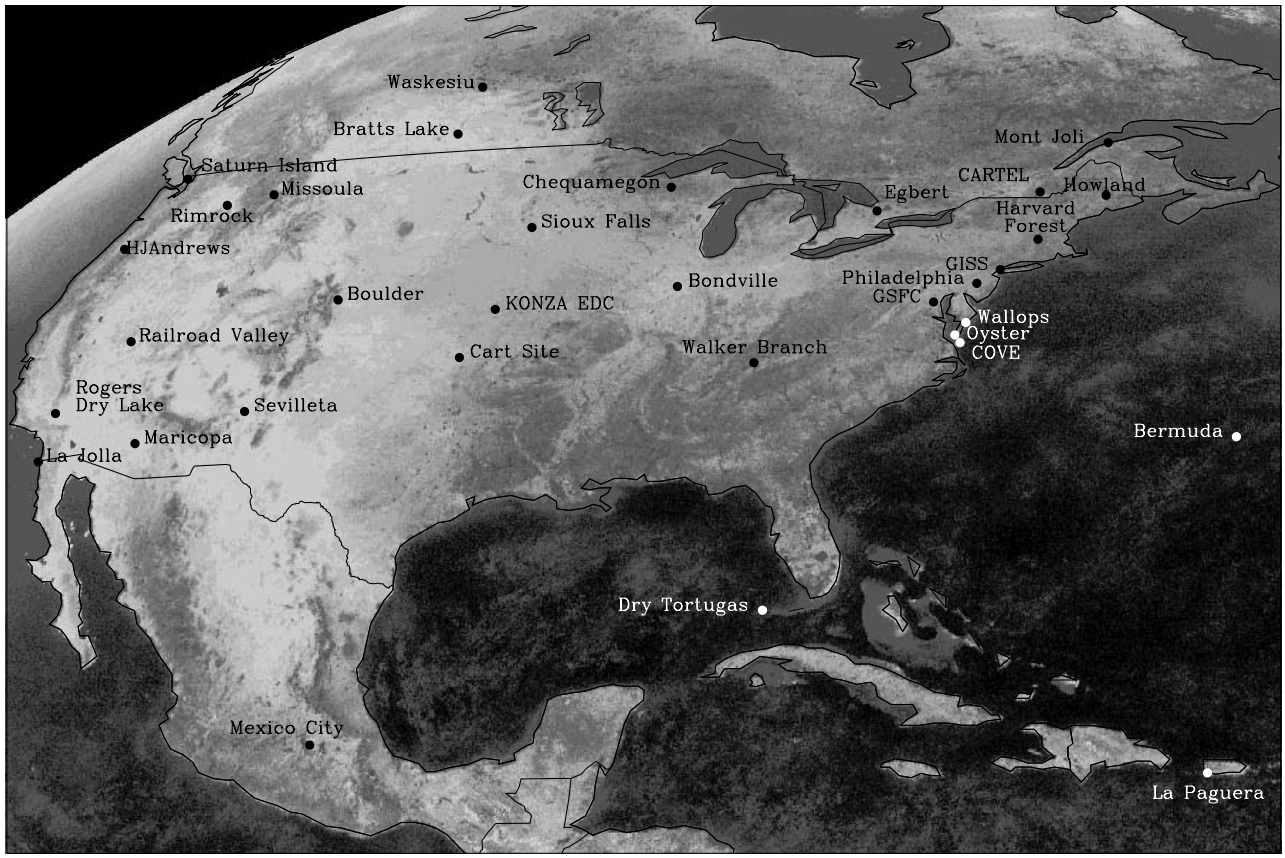

Figure 1. Location of the 33 Aerosol Robotic Network (AERONET) sites used in this study. The background is a cloud-free composite image from GOES 8 visible data demonstrating the varying surface reflectances for the sites investigated.

month. The June-only linear regression (long-dashed lines) shows a lower intercept (because the surface is darker) and a different slope than the July–August linear regression (short-dashed lines); statistics for these comparisons are provided in Table 2. This analysis shows that the aerosol signal during June is significantly different from that during July and August. For each time period in Figure 3, the June Δm is lower than that for all 3 months (compare with Table 2).

[17] Thus it is apparent that changes in the land cover at the Cart Site are affecting the initial 3-month comparisons. Further analysis at Konza EDC and Centre d'Applications et de Recherches en Télédétection (CARTEL, not shown) exhibit similar temporal surface changes, but less so at remaining sites (with no trend evident at sites with little to no vegetation). Thus the following comparisons use all three months to calculate the aerosol signal.

2.4. Observed Aerosol Signal

[18] In Figure 4, the aerosol signal (m, circles) and uncertainty (Δm: vertical lines) are shown for the remaining 32 AERONET sites. The median aerosol signal ($\hat{m}$) and SNR of all comparisons at each site are provided in Table 1. Similar to the Konza site, the aerosol signal at other sites is largest for early and late times, and corresponds to increased multiple scattering as the path length through the atmosphere increases at larger solar zenith angles.

[19] However, the aerosol signal at each AERONET site shows significant variations in how ρ_{sat} responds to changes in τ. While increasing τ corresponds with increasing ρ_{sat} at most sites (i.e., $m > 0$), m is negative at some sites. Particularly, the signal at Maricopa is negative with 71% of the comparisons having $m < 0$ (compare with Table 1). Other sites with negative aerosol signal include Sevilleta, Railroad Valley and CARTEL. While the first three are clearly in the desert southwest where the surface is brighter (compare with Figure 1), it is less obvious why a negative signal occurs for CARTEL. The CARTEL signal shows a minimum in aerosol signal (along with maximums in Δm) near local noon; a similar trend occurs at Harvard Forest and Howland.

[20] This tendency toward larger noise near local noon is explored by comparing SNR to the scattering angle (Θ) from each comparison time at each site (Figure 5). While the result shows large scatter, the median SNR (solid line, binned every 10° in Θ) suggests that the SNR does decrease with increasing Θ. This result is consistent with *Knapp et al.* [2002], who, in estimating GOES τ retrieval uncertainty, show that retrieval errors increase with Θ. The error dependence on scatter angle is likely to result from shorter path lengths for backscatter conditions, the proximity of the observation to the BRDF "hot spot," and variability of the aerosol phase function at these backscatter angles. The largest scattering angles at CARTEL, Harvard Forest, and Howland (i.e., that nearest to local noon) are 151°, 162°, and 154°, respectively. Thus the increase in Δm at these sites can be explained by this scattering angle dependence.

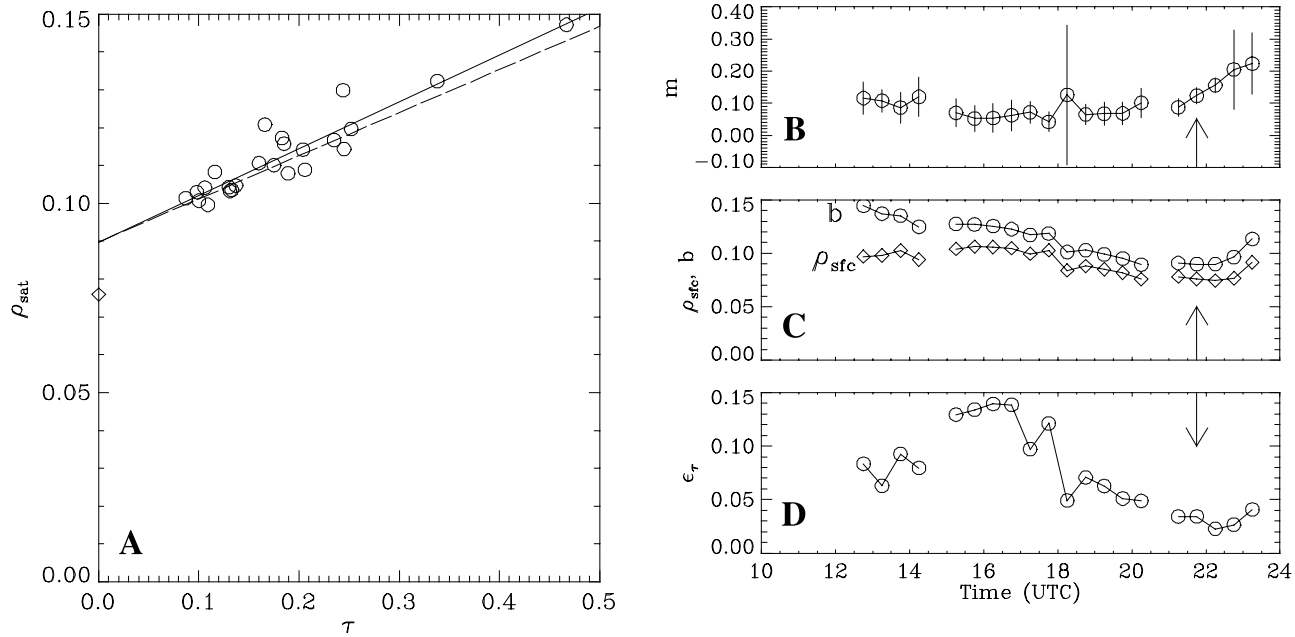

Figure 2. (a) Example comparison of AERONET τ with GOES ρ_{sat} (observations from 2145 UTC from multiple days) with linear regression line (solid line), retrieved surface reflectance (diamond) and water soluble model aerosol signal (dashed line) at Konza EOS Data Center (EDC) AERONET site. Also, (b) the time series of linear regression slope, (c) intercept, and ρ_{sfc} and (d) ε_τ for Konza EDC are provided. (Note that gaps in the time series are due to lack of GOES observations at 1445 and 2045 UTC.) The arrows in Figures 2b, 2c, and 2d denote the linear regression values for the comparison at 2145 UTC (Figure 2a).

[21] Finally, the aerosol signal is quantified using SNR. Where SNR > 1, there is a 99% probability that the aerosol signal detected is not zero, so τ could be retrieved. Of the 33 sites investigated, 25 show an aerosol signal above the noise level for 50% or more of the day (see Table 1). Again, sites in the desert southwest show little aerosol signal and the negative signal at CARTEL is again evident. Also, this analysis shows that there may be problems with retrievals at Boulder and Bratts Lake, having SNR > 1 for only 29 and 21% of the time, respectively. These comparisons of slope with uncertainty show an aerosol signal suggesting potential for an aerosol retrieval at 25 sites, yet: Is the observed aerosol signal realistic?

3. Comparison of Observed Signal With Theory

[22] While the emphasis in the previous section was on detecting the aerosol signal using the signal-to-noise ratio, it is also important to show that the detected signal matches theory. The aerosol signal found in the previous section could be used to develop an empirical aerosol retrieval, but it is important to compare the observed signal

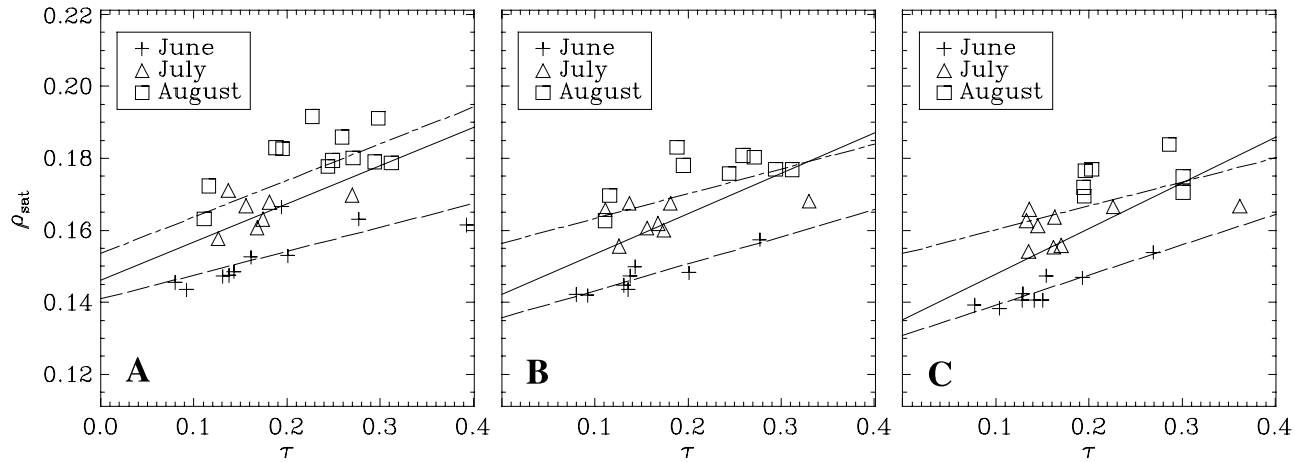

Figure 3. Comparison of GOES ρ_{sat} with AERONET τ and resulting linear regression results for June, July, and August (solid line), June only (dashed line), and July and August (dashed-dotted line) for the Cart Site for (a) 1615, (b) 1645, and (c) 1715 UTC.

Table 2. Comparisons at the Cart Site AERONET Site for Different Months[a]

Time, UTC	Months	n	m	Δm	b
1615	J/J/A	29	0.106	0.071	0.146
1615	J	10	0.066	0.053	0.141
1615	J/A	19	0.101	0.070	0.154
1645	J/J/A	25	0.112	0.074	0.142
1645	J	8	0.075	0.038	0.136
1645	J/A	17	0.069	0.060	0.156
1715	J/J/A	25	0.127	0.077	0.135
1715	J	9	0.084	0.038	0.130
1715	J/A	16	0.066	0.068	0.153

[a] The aerosol signal (m), signal uncertainty (Δm) and linear regression intercept (b) of: June, July, and August (J/J/A), June (J), and July and August (J/A).

to that predicted from radiative transfer to develop a physically based retrieval.

3.1. Modeling Aerosol Signal

[23] The aerosol signal is simulated using the second simulation of the satellite signal in the solar spectrum (6S) radiative transfer model [*Vermote et al.*, 1997], where the response of the simulated satellite-detected reflectance (ρ_{sat}^{6S}) to changing τ is dependent upon numerous parameters. Rayleigh optical depth is estimated by 6S using the altitude of the AERONET site. Ozone absorption is estimated using the average TOMS-retrieved ozone amounts for June through August at each site, while the AERONET observations provide the average column water vapor amount for each comparison. The modeled aerosol signal (m_m) is calculated from

$$m_m = \frac{\Delta\rho_{sat}^{6S}}{\Delta\tau} = \frac{\rho_{sat}^{6S}(\tau = 0.3) - \rho_{sat}^{6S}(\tau = 0.1)}{0.3 - 0.1}. \quad (5)$$

These optical depth values are typical of the range observed at the AERONET sites.

[24] In calculating ρ_{sat}^{6S} a Lambertian surface is assumed. In the comparisons above, the linear regression offset (e.g., Figure 2c) is an estimate of ρ_{sat} when $\tau = 0$, so it is used to retrieve the surface reflectance, ρ_{sfc}. The assumption of a Lambertian surface is relatively accurate given the fixed viewing and illumination geometries available with geostationary orbit. While comparisons with AERONET show effects of the surface BRDF (such as the variation in ρ_{sfc} in Figure 2c), the surface anisotropy causes only a small bias as long as the hot spot region is avoided [*Knapp et al.*, 2002]. The retrieved surface reflectance for Konza EDC at 2145 UTC is 0.076 (diamond in Figure 2a).

[25] The largest uncertainty in calculating the aerosol signal is the estimation of the aerosol optical properties, so a variety of aerosol models are used to estimate a "best fit" model for each site. That is, the aerosol signal is calculated for each comparison time at a site using numerous aerosol models. The aerosol models used are available in the 6S model whose phase functions and single scatter albedos (ω_o) at 0.55 μm are provided in Figure 6. Figure 6a depicts the continental, urban, and maritime models. These are linear combinations of four modes: dust-like, soot-like, water-soluble, and oceanic (Figure 6b). These represent a wide range of ω_o and phase function distributions (which relate to aerosol size). Simulated signals using these models are compared to the observed signal, which is shown for Konza EDC in Figure 7. (Also, note that the aerosol vertical distribution in 6S is exponential in height with a scale height of 2 km.)

3.2. Simulated Signal at Konza EDC

[26] The aerosol signals for different aerosol models show noticeable differences. Most notable is that the more absorbing aerosols (urban, dust-like, and soot-like) show negative aerosol signals, which is consistent with *Kaufman* [1987]. Another difference is the increase in signal for the maritime and oceanic relative to other models from 1500 to 1800 UTC, which deviates from the otherwise decreasing values from sunrise to noon and increasing values from noon to sunset. This results from their lack of absorption ($\omega_o = 0.99$) and increase in scattering from $\Theta = 120°$ to $150°$ (in Figure 6, compare oceanic and maritime phase function with other models). In light of the differences, one similar trend for all aerosol models is the increase in aerosol signal at earlier and later times.

[27] The root-mean-square difference (RMS) is used to compare the fit of simulated aerosol model signals to those observed. It is calculated via

$$\mathrm{RMS} = \sqrt{\frac{\sum(m_m - m)^2}{N}}, \quad (6)$$

where the summation is over N comparisons during the day. For Konza EDC the best fit is the water-soluble model with an RMS = 0.02. The aerosol model signal having the lowest RMS is shown for the other AERONET sites by the triangles in Figure 4. It is apparent that certain sites and regions have better modeled aerosol signal than others.

3.3. Simulated Signal for All Sites

[28] The style of plot in Figure 4 provides a visual estimate toward the likely performance of a τ retrieval for each location. First, times where the signal is uncertain (i.e., large vertical lines) convey that there are changes in ρ_{sat} that do not correspond to changes in τ. For instance, the signal at COVE is generally small (with the median signal, $\hat{m} = 0.072$), but Δm is also small. Conversely, the signal at Bratts Lake is large ($\hat{m} = 0.189$), yet so is Δm. This suggests a retrieval at COVE will be more accurate than at Bratts Lake in spite of its larger signal, which reflects in the SNR differences (compare with Table 1). Second, analysis of Figure 4 aids in determining when the modeled signal is different from that observed. For example, at Wallops the modeled aerosol signal closely matches that observed by GOES (RMS = 0.02). Conversely, the signal at Rimrock (RMS = 0.21) does not correspond with any aerosol model owing to large variations in the signal. This suggests that in spite of the median SNR of 1.3 and SNR > 1 for 63% of the day, τ cannot be retrieved at Rimrock because the signal observed does not match theory. Thus it is possible to determine where a τ retrieval would be most accurate by using both RMS and noise, namely, sites with low RMS and Δm (from Figure 4) or low RMS and large SNR (Table 1).

[29] Such analysis suggests that retrievals will be more accurate for oceanic (e.g., Dry Tortugas, Bermuda) and coastal (e.g., COVE, Wallops) areas, which generally have both low RMS and Δm. The urban sites (i.e., GSFC,

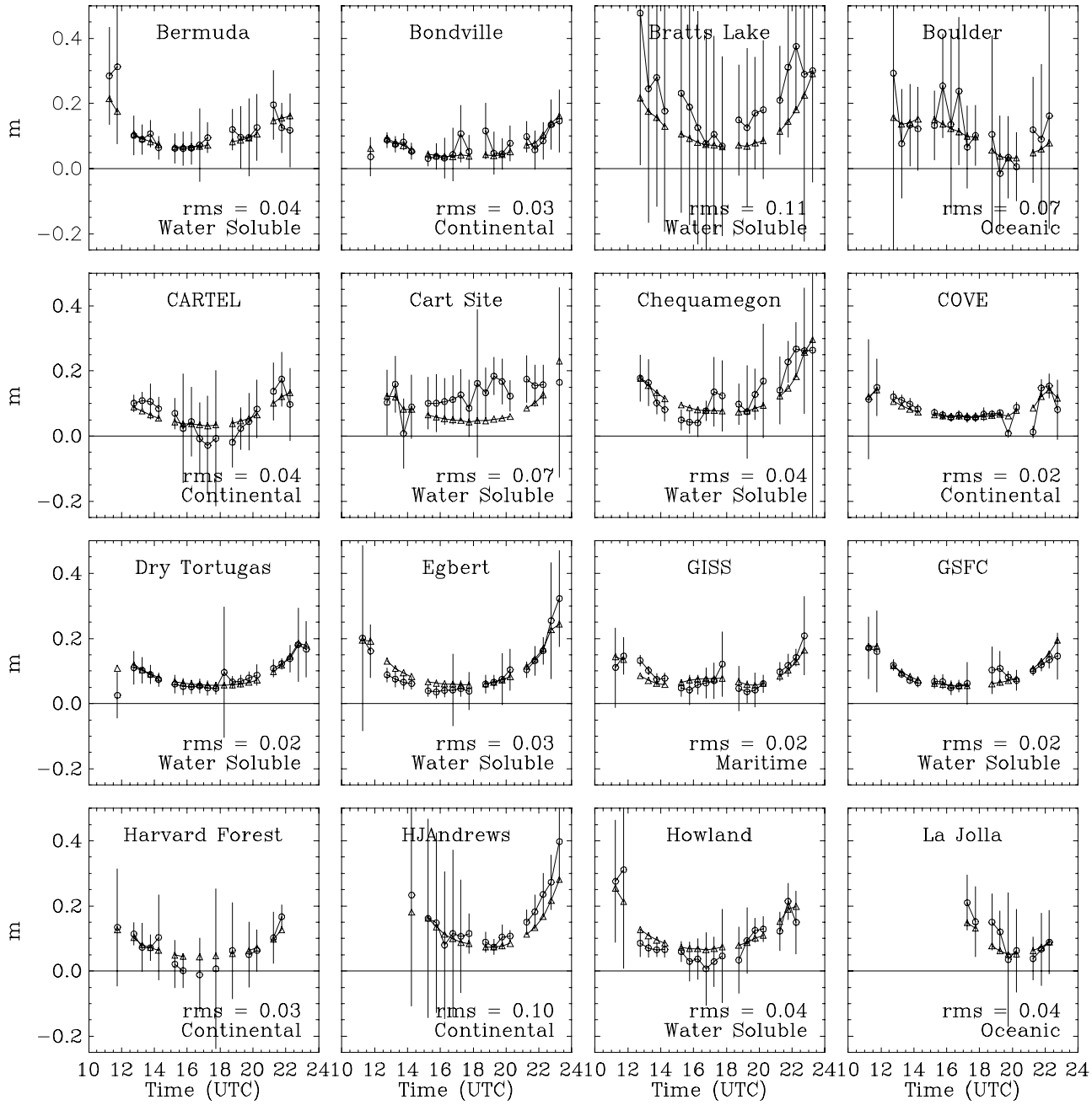

Figure 4. Detected aerosol signal (m) at each site (circles) with Δm, the 99% confidence limit (vertical lines) versus time of day. The simulated signal (m_m) of the best fit model (triangles) is listed with the corresponding root-mean-square difference (RMS). Times when $m \sim m_m$ and Δm is small suggest greater potential for τ retrievals.

Philadelphia, and GISS) also have aerosol signals closely matched by model simulations. Also, while the RMS at Walker Branch is 0.07 (increased due to one noisy comparison at 2245 UTC), the potential for retrieval remains high. This is due to the well-described aerosol signal and small uncertainties at other times.

[30] Vegetated sites show a larger variation in retrieval performance. The northeastern sites (CARTEL, Egbert, Harvard Forest, Howland, and Mont Joli) have comparisons with RMS ranging from 0.03 to 0.04. However, Mont Joli shows trends in observed signal not corresponding to models. Results for CARTEL, Harvard Forest, and Howland show a trend consistent with the scatter angle dependence described above. Vegetated sites farther west (Bondville, Cart Site, Chequamegon, Konza EDC, and Sioux Falls) are in areas of more agriculture usage. These sites have RMS ranging from 0.02 to 0.07 and have slightly larger signal uncertainties. Particularly, the Cart Site shows an observed aerosol signal trend different from the modeled trend, which was found to relate to surface changes (as discussed above). The remaining vegetated sites are at larger view zenith angles.

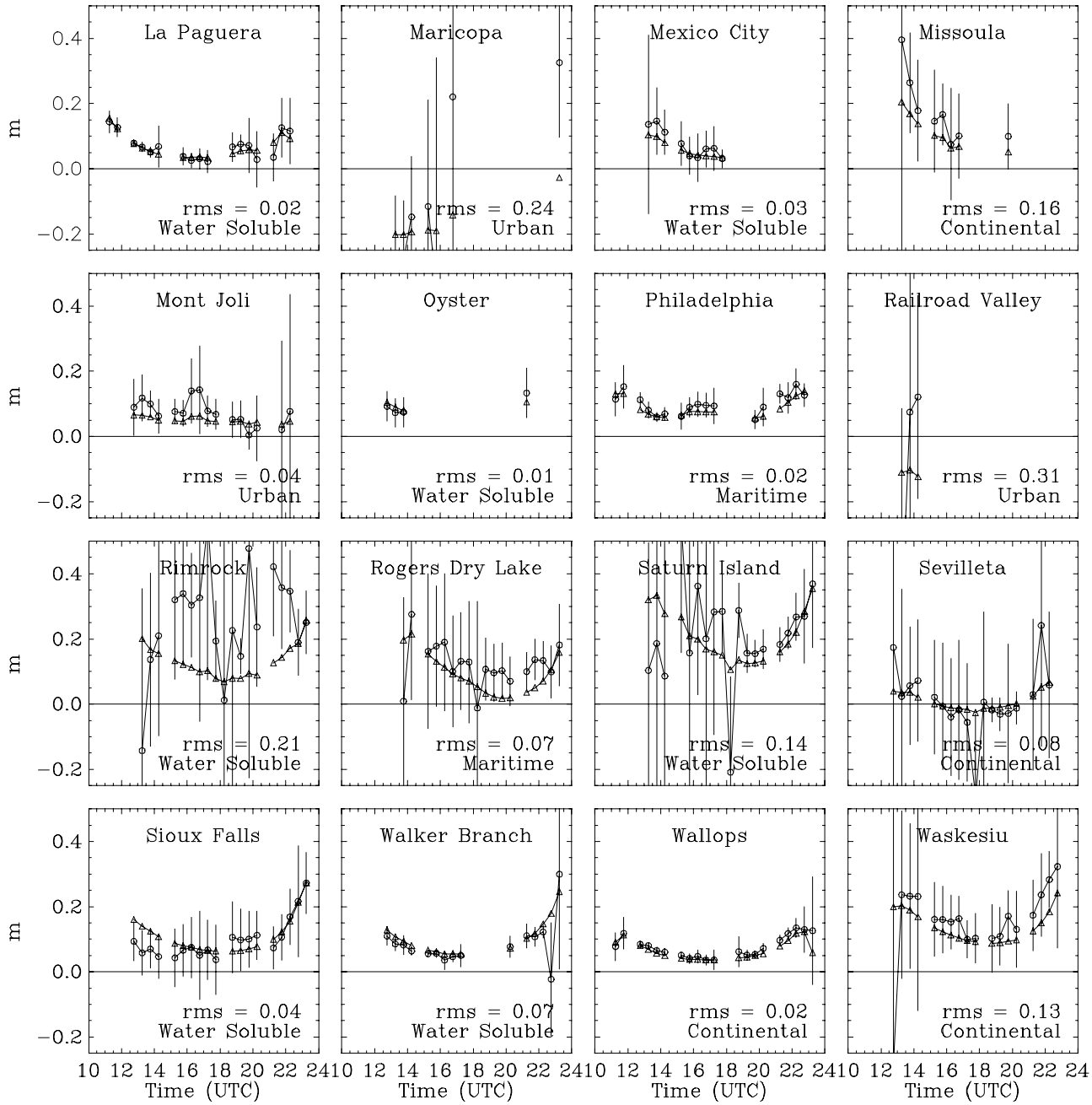

Figure 4. (continued)

[31] The sites in the Pacific Northwest and central Canada also demonstrate a significant possibility for aerosol retrieval in spite of large noise and RMS. HJAndrews, Missoula, Saturn Island, and Waskesiu all show trends of decreasing Δm with time of day (compare with Figure 4). That is, as the sun sets at each site, the aerosol signal becomes more defined (through lower Δm) and follows the simulated signal. This is consistent with lower error for smaller scattering angles (compare with Figure 5) and suggests that retrievals in these regions are possible.

[32] Finally, four sites located in the desert southwest (Maricopa, Railroad Valley, Rogers Dry Lake, and Sevilleta) are the brightest locations in this study ($\hat{\rho}_{sfc} > 0.18$, compare with Table 1). At these sites, the surface signal is much larger than the aerosol signal, which increases Δm. Thus it is unlikely aerosol optical depth could be accurately retrieved at these sites.

[33] Analysis of Figure 4 can be summarized by comparing the median SNR with the RMS (shown in Figure 8 where the names of some outliers are included). Where the SNR is large (particularly, greater than 1) and the RMS is small, there is sufficient aerosol signal, which closely matches theory, to perform a retrieval. However, larger RMS suggests departure from theory while smaller SNR suggests less signal or increasing noise, both of which will decrease the performance of an aerosol retrieval. Again, the oceanic and urban sites are better regions for retrievals while the southwest and those having significant errors near

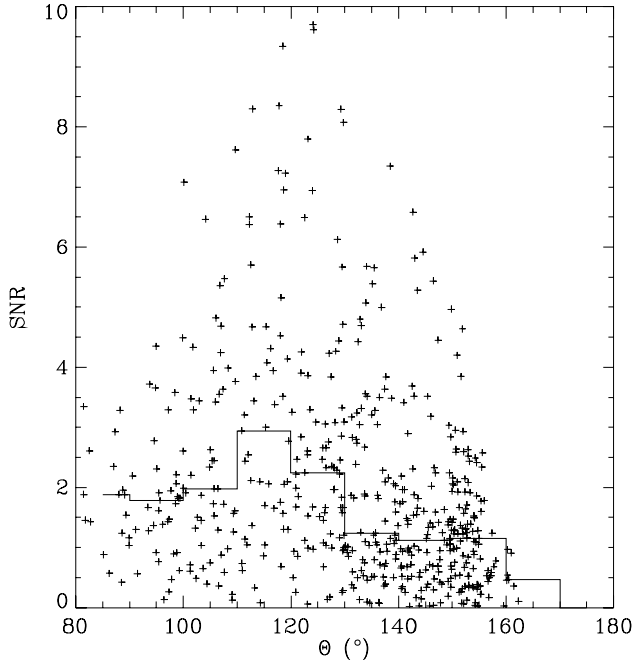

Figure 5. Signal-to-noise ratio, SNR (crosses), versus scattering angle (Θ), with the median SNR every 10° (solid line) showing larger uncertainty near backscatter directions.

local noon (e.g., CARTEL and Harvard Forest) show less potential for an aerosol retrieval.

4. Conclusions

[34] An aerosol signal is present in GOES 8 satellite-detected reflectances at numerous sites around North America. This is determined by comparing calibrated GOES 8 visible observations with AERONET measurements of aerosol optical depth. The sites in this study include regions of the United States, Canada, and Atlantic Ocean with vastly different types of land cover. The observed signal demonstrates the possibility for τ retrievals at all sites except for bright surfaces in the southwestern United States. Error analysis suggests that outside this region, there is sufficient aerosol signal some time during the day for a retrieval.

[35] The comparisons between GOES 8 and AERONET data demonstrate a diurnal trend in aerosol signal, which allows comparison with simulated aerosol signal from a radiative transfer model. Simulated signals compare well with observations at most sites; where an aerosol signal exists, it is often close to theoretical estimates. While variations from theory do occur, they can be partially explained by changes in the surface reflectance due to vegetative changes, as shown for the Cart Site. Also, sites with larger surface reflectances were noisier when compared to theory, showing little potential for aerosol retrieval.

[36] Nonetheless, results show that it is possible to retrieve aerosol optical depth over much of the Unites States and Canada from GOES 8, including ocean and land regions. So, aerosols can be monitored at 15 to 30 min intervals (depending on GOES scheduling), providing timely measurements of aerosols for applications toward wildfire smoke monitoring, pollution transport, and verification of transport models.

[37] Further research should expand results from the AERONET sites to other regions where obtaining ρ_{sfc} will be otherwise complex. While there are two primary methods for retrieving visible wavelength ρ_{sfc}, either using coincident observations at 2.2 μm [*Kaufman et al.*, 1997b] or the compositing of multiple observations to estimate the "clearest" reflectance [*Knapp and Stowe*, 2002; *Knapp et al.*, 2002], only the latter is currently available from geostationary orbit, which raises some questions: For example, how much time is required to observe a "background aerosol signal" from which the surface reflectance can be retrieved? Or, how much change in the surface reflectance is allowable during this time before the errors become too large? In addition to this study, these questions need to be answered to fully understand the uncertainty of the retrieval of aerosol optical depth from geostationary orbit.

[38] The results herein do not, however, detract from the performance or necessity of MODIS, MISR or future polar

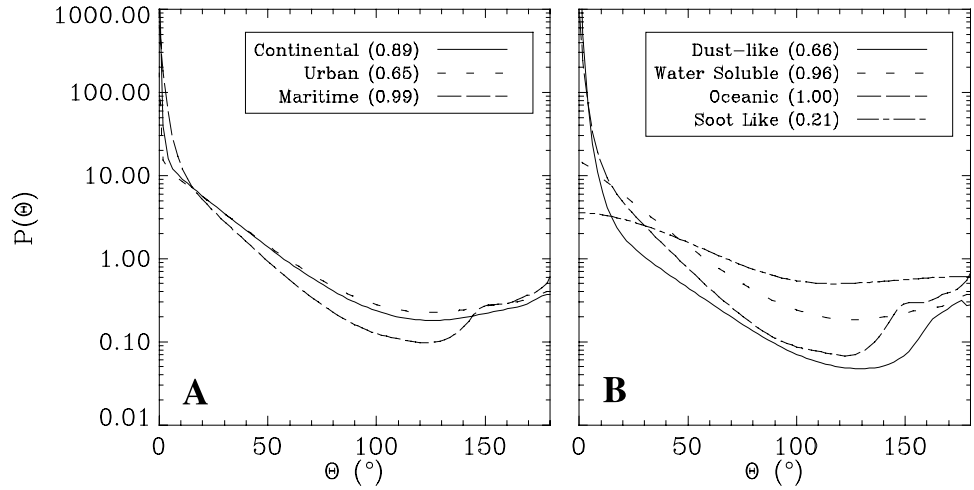

Figure 6. The 6S aerosol model phase function, P(Θ), and ω_o at 0.55 μm for the aerosol signal simulations.

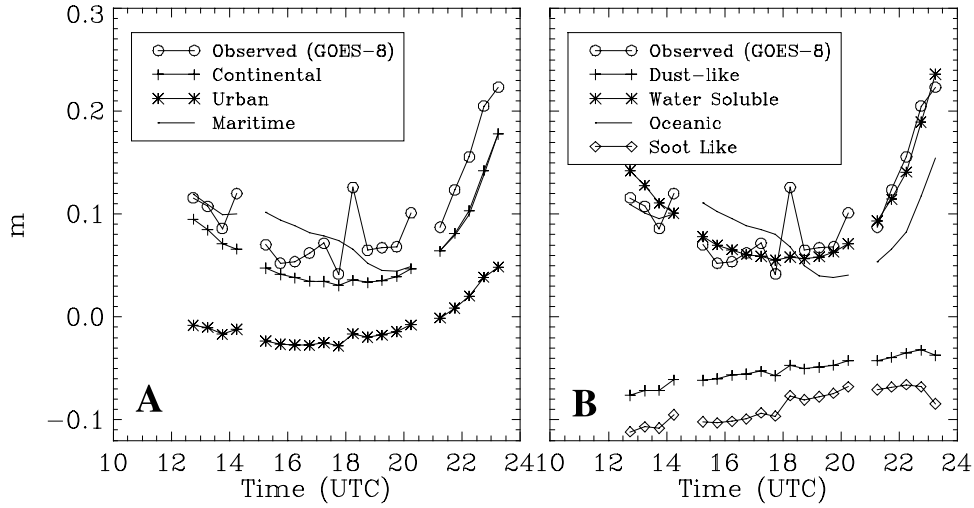

Figure 7. Comparison of the observed aerosol signal (circles) at Konza EDC with simulated signal from different 6S aerosol models.

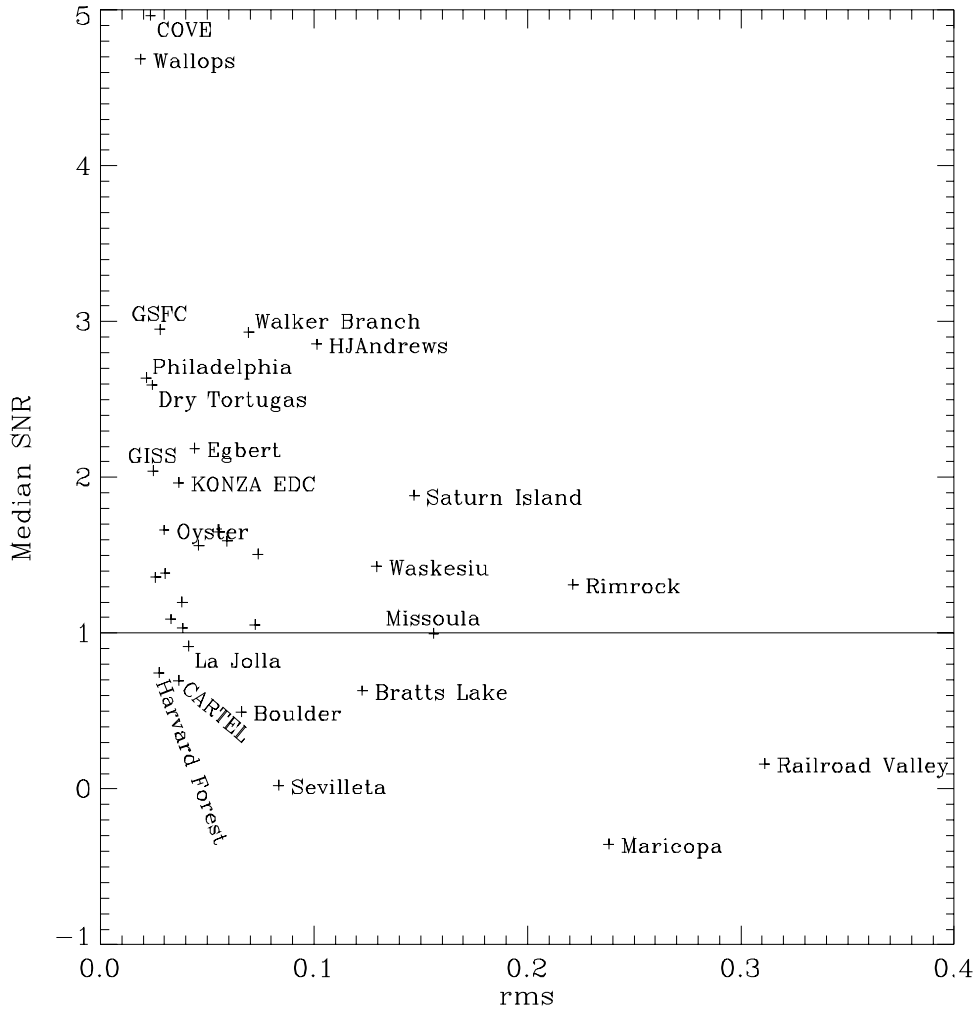

Figure 8. Comparison of the RMS resulting from the simulated versus observed aerosol signal with the median SNR (where names of outlying sites are provided to aid in interpretation). In general, a τ retrieval will be more accurate for sites with lower RMS and larger SNR.

orbiting instruments, which have aerosol detection capabilities enhanced by instrument design. Instead, observations from polar orbiting satellites could enhance the accuracy of the geostationary retrievals by providing daily "calibration" comparisons. These could provide better estimates of the aerosol and surface optical properties, thus increasing the retrieval accuracy.

[39] **Acknowledgments.** The author acknowledges numerous people that have made this research possible through the provision of data. The AERONET is an invaluable resource for this work, therefore I am grateful to Brent Holben (AERONET Project Head), the AERONET staff, and the following principal investigators for making their AERONET data available for this research: Robert Frouin, Mark Helmlinger, Brian Markham, Chuck McClain (SIMBIOS Project Science Team), Dave Meyer, Mark Miller, Norm O'Neill (Canadian AEROCAN network), Kurt Tome, Jeannette Vandenbosch, Anne Vermeulen, Ken Voss, and John Vande Castle. Also, thanks to Peter Romanov for providing access to the GOES data. Finally, this work was supported by the NOAA/National Hazards Information Strategy and the NASA/Global Aerosol Climatology Project (purchase order S-10189X, Michael Mishchenko, Project Scientist). Also, Istvan Laszlo, Robert Frouin and anonymous reviewers have provided valuable advice during the preparation of this manuscript.

References

Bruegge, C. J., R. N. Halthorne, B. L. Markham, M. Spanner, and R. Wrigley, Aerosol optical depth retrievals over the Konza Prairie, *J. Geophys. Res.*, *97*, 18,743–18,758, 1992.

Conel, J. E., Determination of surface reflectance and estimates of atmospheric optical depth and single scattering albedo from Landsat Thematic Mapper data, *Int. J. Remote Sens.*, *11*, 783–828, 1990.

Dubovik, O. V., and M. D. King, A flexible algorithm for retrieval of aerosol optical properties from Sun and sky radiance measurements, *J. Geophys. Res.*, *105*, 20,673–20,696, 2000.

Durkee, P. A., F. Pfeil, E. Frost, and R. Shema, Global analysis of aerosol particle characteristics, *Atmos. Environ.*, *25A*, 2457–2471, 1991.

Ellrod, G., R. V. Achutuni, J. M. Daniels, E. M. Prins, and J. P. Nelson III, An assessment of GOES-8 imager data quality, *Bull. Am. Meteorol. Soc.*, *79*, 2509–2526, 1998.

Flowerdew, R. J., and J. D. Haigh, Retrieval of aerosol optical thickness over land using the ATSR-2 dual-look satellite radiometer, *Geophys. Res. Lett.*, *23*, 351–354, 1996.

Fraser, R. S., Optical thickness of atmospheric dust over Tadzhikistan, *Atmos. Environ.*, *27A*, 2533–2538, 1993.

Fraser, R. S., Y. J. Kaufman, and R. L. Mahoney, Satellite measurements of aerosol mass and transport, *Atmos. Environ.*, *18*, 2577–2584, 1984.

Griggs, M., Satellite observations of atmospheric aerosols during the EOMET cruise, *J. Atmos. Sci.*, *36*, 695–698, 1979.

Herman, J. R., P. K. Bhartia, O. Torres, C. Hsu, C. Seftor, and E. Celarier, Global distribution of UV-absorbing aerosols from Nimbus-7/TOMS data, *J. Geophys. Res.*, *102*, 16,911–16,922, 1997a.

Herman, M., J. L. Deuzé, C. Devaux, P. Goloub, F. M. Bréon, and D. Tanré, Remote sensing of aerosols over land surfaces including polarization measurements and application to POLDER measurements, *J. Geophys. Res.*, *102*, 17,039–17,049, 1997b.

Higurashi, A., T. Nakajima, B. N. Holben, A. Smirnov, R. Frouin, and B. Chatenet, A study of global aerosol optical climatology with two-channel AVHRR remote sensing, *J. Clim.*, *13*, 2011–2027, 2000.

Holben, B. N., et al., AERONET - A federated instrument network and data archive for aerosol characterization, *Remote Sens. Environ.*, *66*, 1–16, 1998.

Kachigan, S. K., *Statistical Analysis*, 589 pp., Radius, New York, 1986.

Kaufman, Y. J., Satellite sensing of aerosol absorption, *J. Geophys. Res.*, *92*, 4307–4317, 1987.

Kaufman, Y. J., D. Tanré, L. A. Remer, E. F. Vermote, A. Chu, and B. N. Holben, Operational remote sensing of tropospheric aerosol over land from EOS moderate resolution imaging spectroradiometer, *J. Geophys. Res.*, *102*, 17,051–17,067, 1997a.

Kaufman, Y. J., A. E. Wald, L. A. Remer, B.-C. Gao, R.-R. Li, and L. P. Flynn, Remote sensing of aerosol over the continents with the aid of a 2.2 μm channel, *IEEE Trans. Geosci. Remote Sens.*, *35*, 1286–1298, 1997b.

Kaufman, Y. J., B. N. Holben, D. Tanré, I. Slutsker, A. Smirnov, and T. F. Eck, Will aerosol measurements from Terra and Aqua polar orbiting satellites represent the daily aerosol abundance and properties?, *Geophys. Res. Lett.*, *27*, 3861–3864, 2000.

King, M. D., Y. J. Kaufman, D. Tanré, and T. Nakajima, Remote sensing of tropospheric aerosols from space: Past, present and future, *Bull. Am. Meteorol. Soc.*, *80*, 2229–2259, 1999.

Knapp, K. R., and L. L. Stowe, Evaluating the potential for retrieving aerosol optical depth over land from AVHRR Pathfinder Atmosphere data, *J. Atmos. Sci.*, *59*, 279–293, 2002.

Knapp, K. R., and T. H. Vonder Haar, Calibration of the eighth Geostationary Observational Environmental Satellite (GOES-8) imager visible sensor, *J. Atmos. Oceanic Technol.*, *17*, 1639–1644, 1999.

Knapp, K. R., T. H. Vonder Haar, and Y. J. Kaufman, Aerosol optical depth retrieval from GOES-8: Uncertainty study and retrieval validation over South America, *J. Geophys. Res.*, *107*(D7), 4055, doi:10.1029/2001JD000505, 2002.

Legrand, M., J. J. Bertrand, M. Desbois, L. Menenger, and Y. Fouqart, The potential of infrared satellite data for the retrieval of Saharan-dust optical depth over Africa, *Adv. Atmos. Sci.*, *28*, 309–318, 1989.

Lyons, W. A., J. C. Dooley Jr., and K. T. Whitby, Satellite detection of long-range pollution transport and sulfate aerosol hazes, *Atmos. Environ.*, *12*, 621–631, 1977.

Menzel, W. P., and J. F. W. Purdom, Introducing GOES-I: The first of a new generation of geostationary operational environmental satellites, *Bull. Am. Meteorol. Soc.*, *75*, 757–781, 1994.

Mishchenko, M. I., and L. D. Travis, Satellite retrieval of aerosol optical properties over the ocean using polarization as well as intensity of reflected sunlight, *J. Geophys. Res.*, *102*, 16,989–17,013, 1997.

Norton, C. C., F. R. Mosher, B. Hinton, D. W. Martin, D. Santek, and W. Kuhlow, A model for calculating desert turbidity over the oceans from geostationary satellite data, *J. Appl. Meteorol.*, *19*, 633–644, 1980.

Stowe, L. L., R. M. Carey, and P. P. Pellegrino, Monitoring the Mt. Pinatubo aerosol layer with NOAA/11 AVHRR data, *Geophys. Res. Lett.*, *19*, 159–162, 1992.

Tsonis, A. A., and W. R. Leaitch, Minimum detectable pollution levels from satellite imagery, *Geophys. Res. Lett.*, *13*, 56–59, 1986.

Veefkind, J. P., and G. de Leeuw, A new algorithm to determine the spectral aerosol optical depth from satellite radiometer measurements, *J. Aerosol Sci.*, *29*, 1237–1248, 1998.

Vermote, E. F., D. Tanré, J. L. Deuzé, M. Herman, and J.-J. Morcrette, Second simulation of the satellite signal in the solar spectrum, 6S: An overview, *IEEE Trans. Geosci. Remote Sens.*, *35*, 675–686, 1997.

Zhang, J., and S. A. Christopher, Intercomparison of smoke aerosol optical thickness derived from GOES 8 imager and ground-based Sun photometers, *J. Geophys. Res.*, *106*, 7387–7397, 2001.

Zhao, T. X.-P., L. L. Stowe, A. Smirnov, D. Crosby, J. Sapper, and C. R. McClain, Development of a global validation package for satellite oceanic aerosol retrieval based on AERONET Sun-photometer observations and its application to NOAA/NESDIS operational aerosol retrievals, *J. Atmos. Sci.*, *59*, 294–312, 2002.

K. R. Knapp, NOAA/NESDIS/ORA/CIRA, Room 711, 5200 Auth Road, Camp Springs, MD 20746-4304, USA. (Ken.Knapp@noaa.gov)